

EFFECTS OF NON-ISOTHERMAL OXIDATION ON TRANSIENT CONJUGATE HEAT TRANSFER OF THE CRYO-SUPERSONIC AIR-QUENCHING

by

**Jian YANG^{a,b}, Yue ZHANG^b, Mingxin GAO^c,
and Hua SONG^{a,b*}**

^a School of Materials and Metallurgy, University of Science and Technology Liaoning,
Anshan, China

^b School of Mechanical Engineering and Automation,
University of Science and Technology Liaoning, Anshan, China

^c Engineering Training Center, University of Science and Technology Liaoning,
Anshan, China

Original scientific paper

<https://doi.org/10.2298/TSCI201111147Y>

In this paper, the effects of non-isothermal oxidation on transient conjugate heat transfer of the cryo-supersonic air-quenching are investigated based on a double-layered oxidation kinetics model, while a unified conjugate heat transfer formula is developed to synthetically consider the near-wall turbulence, non-isothermal oxidation, and surface radiation. The comparison between numerical and experimental results are also presented to check the validity of the developed model. The results indicate that the film growth has some degree of inhibition to the conjugate heat transfer, in particular, the stagnation temperature increases linearly by about 5 K per 100 μm increase in film thickness, and the effective conjugate heat transfer coefficient in the stagnation region decreases linearly by about 55 $\text{Wm}^{-2}\text{K}^{-1}$ per 100 μm increase in film thickness. Moreover, the oxide film would have little impact on transient conjugate heat transfer when the near-wall velocity is higher due to the effect of viscous dissipation.

Key words: conjugate heat transfer, air-quenching, non-isothermal oxidation, transient

Introduction

Forced air-quenching technology is widely used in the heat treatment process of rail, steel slag, glass sheet, and aluminum alloy due to its green quenchant and good cooling uniformity [1-3]. As an improvement, the cryo-supersonic air-quenching can be achieved by means of the compressed air and Laval nozzle for higher cooling speed and larger scale application. But because of the open environment, the presence of oxygen in the air will inevitably induce the high temperature oxidation of the workpiece. The formed oxide film with certain thermal resistance would have an important impact on heat transfer [4-6]. During the cooling process of the cryo-supersonic air-quenching, the non-isothermal growth of the oxide film with varying interfacial temperature and oxygen partial pressure would lead to more complex transient conjugate heat transfer. Thus, based on our earlier work with constant film thickness Yang *et al.* [7], the specific heat transfer phenomenon induced by the oxidation kinetics needs to be further studied.

* Corresponding author, e-mail: songhua88@126.com

In practice, the heat transfer process with oxide film is very common in industrial production, while many experimental and theoretical researches have been conducted to address such problems. Xu *et al.* [8] investigated the wall temperature profiles of the superheater and reheater tubes in the power plant by considering a single-layer oxide film with uniform thickness, and the effect of film thickness on the wall temperature was analyzed. The thermal conductivity between the oxide film and the tube wall metal was calculated using the harmonic mean method. Qi *et al.* [9] utilized the CFD technique and analytical method to simulate the steady-state heat transfer of the superheater tubes. For the superheater tube with the ash deposit or steam-side oxide film, the outer tube wall temperature was assessed by the thermal resistance method. The oxide film was assumed to be a single layer with thickness taken as the mean value of the measured results. Li and Sellars [10] provided an analysis of the interfacial heat transfer during the hot axisymmetric forging and flat rolling experiments of plain carbon steel with oxide film formation, the interfacial heat transfer mechanisms under different conditions were obtained, which indicated that the continuous oxide film formed by adhesive friction in hot forging exhibited relatively high thermal resistance. Wu *et al.* [11] carried out the theoretical analysis of interfacial heat transfer of strip rolling under different contact conditions, in which the thickness and thermal conductivity of the oxide film were considered by a modified interfacial heat transfer coefficient. Hu *et al.* [12] developed an optimization-based approach for the impact analysis of temperature, contact pressure and oxide film thickness on heat transfer in the hot stamping process. The thermal properties of the oxide film were introduced into the effective heat transfer coefficient that can be obtained by the experiment. Similarly, the concept of the effective heat transfer coefficient was introduced by Chabičovský *et al.* [13] in the impact analysis of oxide film on the Leidenfrost temperature during the spray cooling. Fukuda *et al.* [14] adopted the artificial oxide film with different thicknesses, achieved by the thermal spraying with Al_2O_3 powder, to investigate the effects of oxide film on heat transfer characteristics of the subsonic air jet cooling.

However, it's worth noting that the formed metal oxide during the high temperature oxidation is generally a multilayer structure with film growth, thus the modeling of the oxide film requires special treatment. Wikstrom *et al.* [15] developed a mathematical model for the impact analysis of oxide film on heat transfer of low carbon steel in a reheating furnace, in which the simplified linear and parabolic oxidation formulas were used to consider the film growth based on the isothermal experiment and CFD simulation. Wendelstorf *et al.* [5] experimentally studied the effects of the oxide film and its removal on heat transfer of the spray cooling. The oxidation kinetics for different steel grades was employed to determine the film thickness during the short-time oxidation. Then the effective heat transfer coefficient was estimated based on the obtained film thickness under the assumption of a stable oxide layer. At present, although the effects of oxide film on heat transfer in superheater and reheater tube, hot forging, rolling and stamping, steel reheating, and jet cooling have been extensively studied, the consideration of non-isothermal growth of the multilayer oxide film with varying interfacial temperature and oxygen partial pressure is obviously insufficient, especially in the cryo-supersonic air-quenching.

In the present contribution, the double-layered oxidation kinetics model [16] is employed to determine the instantaneous film growth during the quenching process, taking better account of the varying interfacial temperature and oxygen partial pressure. Then a unified formula is developed to deal with the complex transient conjugate heat transfer with the near-wall turbulence, non-isothermal oxidation and surface radiation. On this basis, the effects of film growth and initial film thickness on transient conjugate heat transfer of the cryo-

supersonic air-quenching are further investigated, in an attempt to understand the heat transfer mechanism induced by the oxide film.

Physical and numerical model

Geometry and governing equations

The geometry of the cryo-supersonic air-quenching of a metal disk with double-layered oxide film is shown in fig. 1. The ξ_1 and ξ_2 are the thickness of Fe_3O_4 and FeO in the oxide film, respectively, p_0 , p_1 , and p_2 are the oxygen partial pressures at $\text{O}_2/\text{Fe}_3\text{O}_4$, $\text{Fe}_3\text{O}_4/\text{FeO}$, and $\text{FeO}/\text{substrate}$ interfaces, respectively. The whole computational domain is marked with solid red lines.

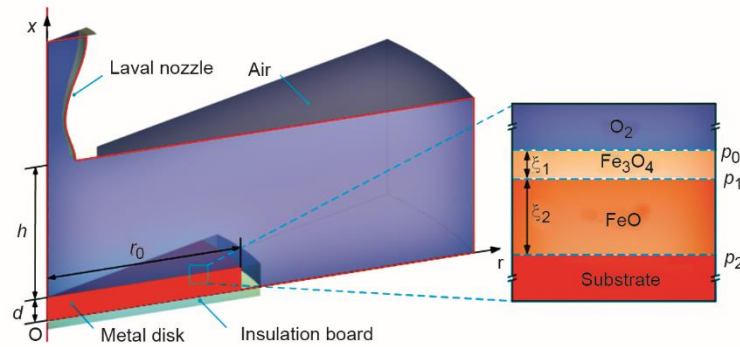


Figure 1. Geometric of the cryo-supersonic air-quenching of a metal disk with oxide film
 (for color image see journal web site)

Non-isothermal oxidation kinetics

Given the important influence of oxide film on heat transfer [1-3], the double-layered parabolic oxidation kinetic model presented by Yurek *et al.* [16] is employed to consider the non-isothermal oxidation during the cryo-supersonic air-quenching. The rate of thickening of the oxide film is given by:

$$\frac{d\xi_{\text{film}}}{dt} = \frac{k_{\text{film}}}{\xi_{\text{film}}} \quad (1)$$

where ξ_{film} is the thickness of the oxide film and k_{film} – the parabolic rate for the diffusion-controlled growth of the entire oxide film, determined by:

$$k_{\text{film}} = \frac{\left(1 + \frac{\xi_2}{\xi_1}\right)^2}{1 + \frac{\xi_2 V_1}{V_2 \xi_1}} k_1, \quad \frac{\xi_2}{\xi_1} = \frac{k_2 V_1}{k_1 V_2} \quad (2)$$

where V_1 and V_2 are the average molar volumes of Fe_3O_4 and FeO , respectively, ($V_1 = 11.7 \text{ cm}^3/\text{mol}$, $V_2 = 11.2 \text{ cm}^3/\text{mol}$) and k_1 and k_2 [cm^2s^{-1}] are the parabolic rates for the growth of Fe_3O_4 and FeO , respectively, defined by:

$$k_1 = \frac{1}{2a} \int_{p_1}^{p_0} D_1 d(\ln p_{\text{O}_2}), \quad k_2 = \frac{1}{2b} \int_{p_2}^{p_1} D_2 d(\ln p_{\text{O}_2}) \quad (3)$$

where $a = 3/4$ for Fe_3O_4 , $b = 1$ for FeO . The D_1 and D_2 [cm^2s^{-1}] represent the self-diffusion coefficients of Fe cations in Fe_3O_4 and FeO , respectively, which can be fitted by the exponential function [17]:

$$D_1 = 0.337f \exp\left(-\frac{227192.028}{RT}\right), \quad D_2 = 0.1667f \exp\left(-\frac{127524.512}{RT}\right) \quad (4)$$

where f is the additional correction factor introduced for steel ($= 0.25$) and R – the molar gas constant ($= 8.314 \text{ J/molK}$). The interfacial oxygen partial pressures [atm] are given by [16]:

$$p_0 = \frac{0.21p_w}{f_p}, \quad \log p_1 = 13.027 - \frac{32797.409}{T}, \quad \log p_2 = 6.529 - \frac{27269.439}{T} \quad (5)$$

where f_p is the conversion coefficient of pressure ($= 1.01 \cdot 10^5 \text{ Pa}$). By dividing the non-isothermal temperature profile into n isothermal intervals, the entire film thickness with initial value ξ_0 can be acquired by integrating eq. (1) over time t :

$$\xi_{\text{film}} = \sqrt{\xi_0^2 + \sum_{i=1}^n [2k_{\text{film}}(T_i)\Delta t_i]} \quad (6)$$

A unified formula for transient conjugate heat transfer

During the cryo-supersonic air-quenching, there exists a complex heat transfer phenomenon implying the supersonic turbulent flow, non-isothermal oxidation growth, and surface radiation at the fluid-solid conjugate interface. The local mesh configuration at the conjugate interface with double-layered oxide film is shown in fig. 2. Given that the complex configuration of the Laval nozzle contour, the orthogonal curvilinear coordinates (ξ, η) are recommended to handle the fluid flow and heat transfer.

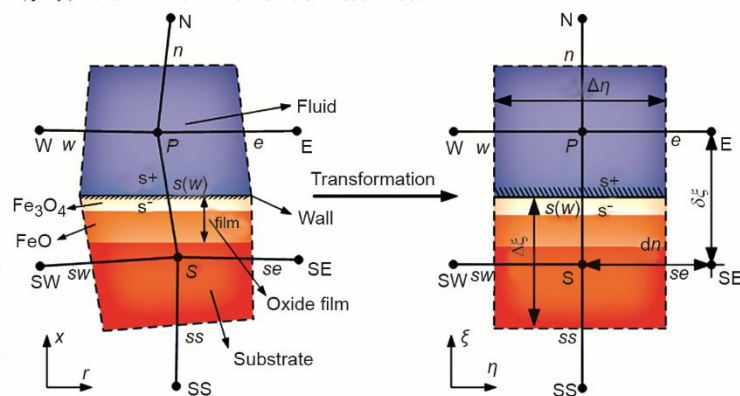


Figure 2. Mesh configuration at the conjugate interface with double-layered oxide film

To efficiently solve the complex transient conjugate heat transfer, the effects of the near-wall turbulence, non-isothermal oxidation, and surface radiation are equivalently introduced into the wall thermal conductivity. Based on this treatment, a unified conjugate heat transfer formula in the orthogonal curvilinear co-ordinates is developed to uniformly deal with the problem of transient conjugate heat transfer of the cryo-supersonic air-quenching.

According to the principle of equal heat flux at the conjugate interface, the following relation exists:

$$q_w = -\lambda_p^{eq} \frac{\partial T}{\partial n} \Big|_{s^+} = -\lambda_s^{eq} \frac{\partial T}{\partial n} \Big|_{s^-} = -\lambda_w^{eq} \frac{\partial T}{\partial n} \Big|_s \quad (7)$$

where q_w is the total wall heat flux, λ_w^{eq} , λ_p^{eq} , and λ_s^{eq} are the equivalent thermal conductivity of the wall, wall-adjacent fluid, and wall-adjacent solid, respectively. By expanding eq. (7) we can obtain:

$$q_w = \frac{T_w - \tilde{T}_p}{\frac{\chi_p}{\lambda_p^{eq}}} = \frac{\tilde{T}_s - T_w}{\frac{\chi_s}{\lambda_p^{eq}}} = \frac{\tilde{T}_s - \tilde{T}_p}{\frac{\chi_p + \chi_s}{\lambda_w^{eq}}} \quad (8)$$

in which

$$\tilde{T}_p = T_p + \left(\frac{T_\eta \beta}{\alpha} \right)_{s^+}, \quad \tilde{T}_s = T_s - \left(\frac{T_\eta \beta}{\alpha} \right)_{s^-}, \quad \chi_p = \left(\frac{J}{\sqrt{\alpha}} \right)_{s^+}, \quad \chi_s = \left(\frac{J}{\sqrt{\alpha}} \right)_{s^-} \quad (9)$$

then, using the previous relations, the wall temperature is given by:

$$T_w = \frac{\frac{\tilde{T}_p \chi_s}{\lambda_s^{eq}} + \frac{\tilde{T}_s \chi_p}{\lambda_p^{eq}}}{\frac{\chi_s}{\lambda_s^{eq}} + \frac{\chi_p}{\lambda_p^{eq}}} \quad (10)$$

Furthermore, considering that the wall heat transfer is mainly contributed by convection, conduction and radiation, the total wall heat flux can also be written as [18-20]:

$$q_w = q_c + q_r = \frac{\rho c_p C_\mu^{1/4} k^{1/2} (T_w - T_p) - D}{T^+} + \varepsilon_r \sigma_r (T_w^4 - T_p^4) \quad (11)$$

where c_p is the specific heat, C_μ – the turbulent viscosity coefficient, k – the turbulence kinetic energy, T^+ – the non-dimensional temperature, and D – the contribution of viscous heating. The ε_r and σ_r denote the emissivity and the Stefan-Boltzmann constant, respectively. By combining eqs. (8)-(11), the equivalent thermal conductivity of the wall-adjacent fluid is computed:

$$\lambda_p^{eq} = \frac{(T_w - T_p)(\rho c_p C_\mu^{1/4} k^{1/2} - D) \chi_p}{T^+ (T_w - \tilde{T}_p)} + \frac{\varepsilon_r \sigma_r \chi_p (T_w^4 - T_p^4)}{T_w - \tilde{T}_p} \quad (12)$$

Based on the equivalent thermal conductivity of the wall-adjacent fluid, the near-wall turbulent flow can be equivalently converted to the laminar flow, while the effect of surface radiation on conjugate heat transfer can also be included. Furthermore, according to the principle of thermal resistance series, the effects of non-isothermal oxidation on transient conjugate heat transfer can be considered by an equivalent method without occupying any grid points, similar to the introduced effective heat transfer coefficient [11-13]. Then the total thermal resistance at the conjugate interface can be represented by:

$$\frac{\chi_P + \chi_S}{\lambda_w^{\text{eq}}} = \frac{\chi_P}{\lambda_P^{\text{eq}}} + \frac{\chi_S}{\lambda_S^{\text{eq}}} = \frac{\chi_P}{\lambda_P^{\text{eq}}} + \frac{\chi_S - \xi_{\text{film}}}{\lambda_S} + \frac{\xi_{\text{film}}}{\lambda_{\text{film}}^{\text{eq}}} \quad (13)$$

Thus the equivalent wall thermal conductivity is computed:

$$\lambda_w^{\text{eq}} = \frac{\lambda_S \lambda_P^{\text{eq}} \lambda_{\text{film}}^{\text{eq}} (\chi_P + \chi_S)}{\lambda_S \lambda_P^{\text{eq}} \xi_{\text{film}} + \lambda_P^{\text{eq}} \lambda_{\text{film}}^{\text{eq}} (\chi_S - \xi_{\text{film}}) + \lambda_S \lambda_{\text{film}}^{\text{eq}} \chi_P}, \quad \lambda_{\text{film}}^{\text{eq}} = \frac{(\xi_1 + \xi_2) \lambda_1 \lambda_2}{\xi_2 \lambda_1 + \xi_1 \lambda_2} \quad (14)$$

where λ_1 and λ_2 are the thermal conductivity of Fe_3O_4 and FeO , respectively. Based on eq. (8), the total heat flow through the wall can be expressed:

$$Q_w = \frac{\tilde{T}_S - \tilde{T}_P}{\frac{\chi_P + \chi_S}{\lambda_w^{\text{eq}}}} A_w = \lambda_w^{\text{eq}} \left(r \frac{\alpha}{J} \right)_s (T_S - T_P) - \lambda_w^{\text{eq}} \left(r \frac{\beta}{J} \right)_s (T_\eta)_s \quad (15)$$

When adding the total wall heat flow, Q_w , into the compact finite volume discretization of the governing equation of transient conjugate heat transfer of the cryo-supersonic air-quenching, the south coefficient, A_S , and the north coefficient, A_N , can be equivalently transformed to:

$$A_S = \lambda_w^{\text{eq}} \left(r \frac{\alpha}{J} \right)_s, \quad A_N = \lambda_w^{\text{eq}} \left(r \frac{\alpha}{J} \right)_n \quad (16)$$

By applying this method, there is no need to impose the additional source terms in the discretization equation for transient conjugate heat transfer, while the effects of the near-wall turbulent flow, high temperature oxidation, and surface radiation can be naturally and uniformly taken into account. The numerical model is implemented by an in-house FORTRAN code, and the obtained results are processed by an in-house MATLAB code.

Model verification

To confirm the validity of the developed model, both the numerical and experimental examples of the cryo-supersonic air-quenching of a Q235 disk ($r_0 = 80$ mm, $d = 15$ mm, and $h = 60$ mm) are investigated. For numerical calculation, the total pressure and temperature at the inlet of the Laval nozzle are set to $0.7 \cdot 10^6$ Pa and 350 K, respectively. The initial temperatures of the fluid domain and solid domain are set as 300 K and 1173.15 K, respectively. The thermal conductivity of Fe_3O_4 and FeO is taken as 3.7 W/mK and 7.5 W/mK, respectively [21]. The experimental apparatus of the cryo-supersonic air-quenching is shown in fig. 3. The key steps are carefully designed:

- Spraying the high-temperature resistant insulation paint onto the bottom and side of the metal disk.
- Placing the metal disk inside the base and top insulation boards and putting them into the resistance furnace.
- Vacuuming the resistance furnace and filling it with the inert gas argon.
- Taking out the metal disk after heating, then quenching the disk immediately after removing the top insulation board.
- Recording the surface temperatures by the infrared thermometers.
- Terminating the experiment when it is on the pre-set time and simultaneously putting the metal disk into the vacuum bucket.
- Vacuuming the bucket and filling it with argon at a certain negative pressure.

- Taking out the cooled disk to prepare the metallographic specimens at different radial positions.
- Measuring the oxide film thickness by the optical microscope.

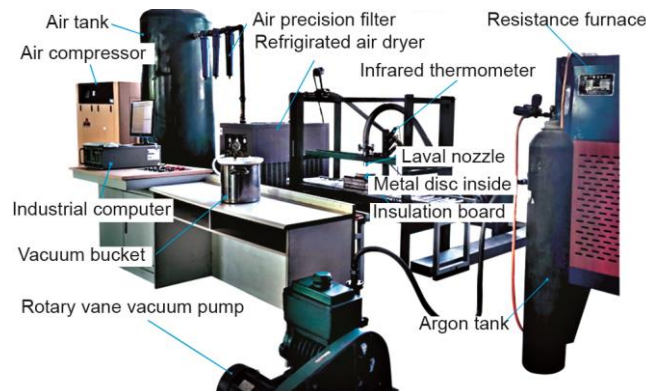


Figure 3. Experimental apparatus of the cryo-supersonic air-quenching

Taking the radial positions $r = 0$ mm, 20 mm, 40 mm, and 60 mm, for example, the comparison between the measured and calculated temperature profiles is shown in fig. 4. It is evident that the calculated results are well consistent with the measured data, with acceptable maximum relative deviations of 8.96%, 7.59%, 5.66%, and 9.17%, respectively. The compar-

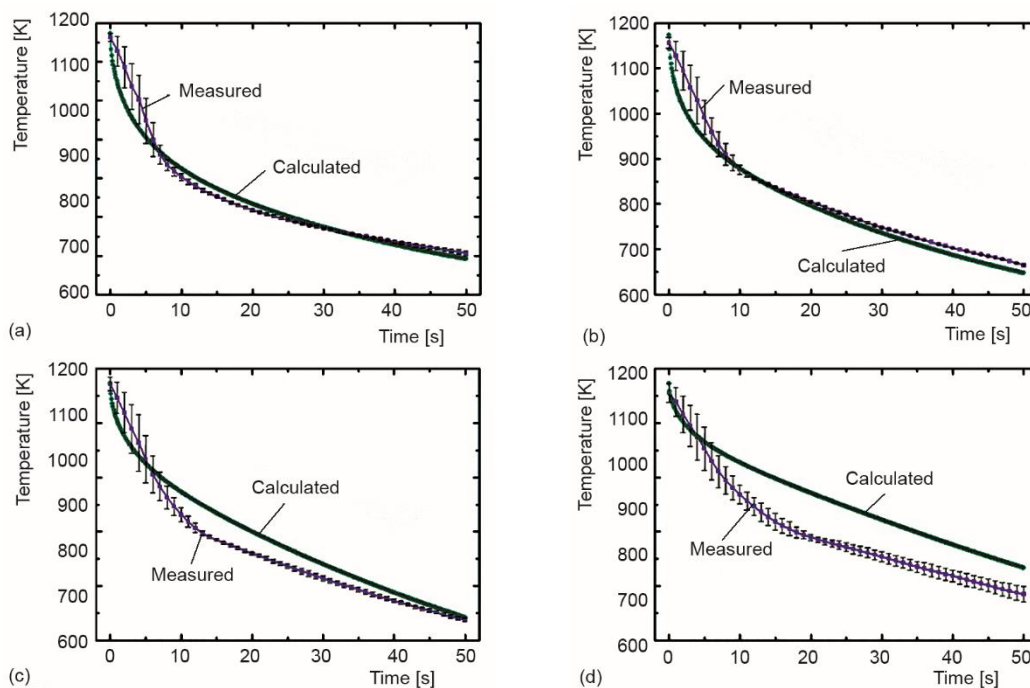


Figure 4. Comparisons of calculated and measured temperatures; (a) $r = 0$ mm, (b) $r = 20$ mm, (c) $r = 40$ mm, and (d) $r = 60$ mm

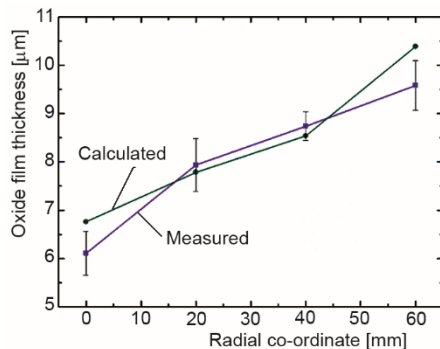


Figure 5. Comparison of calculated and measured film thickness

ison between the calculated and measured film thickness is shown in fig. 5. The relative deviations of the film thickness at different radial positions are 10.68%, 1.91%, 2.30%, and 8.40%, respectively, with a reasonable agreement. The results indicate that the developed model is feasible for impact analysis of transient conjugate heat transfer of the cryo-supersonic air-quenching.

Results and discussions

To facilitate the impact analysis of film growth on transient conjugate heat transfer, the concept of an effective convective heat transfer coefficient (ECHTC), α_{eff} , is introduced. According to Newton's Law of cooling and the total wall heat flux in eq. (8), α_{eff} can be defined:

$$\alpha_{\text{eff}} = \frac{q_w}{\tilde{T}_S - \tilde{T}_P} = \frac{\lambda_w^{\text{eff}}}{\chi_P + \chi_S} = \frac{\lambda_S \lambda_P^{\text{eq}} \lambda_{\text{film}}^{\text{eq}}}{\lambda_S \lambda_P^{\text{eq}} \xi_{\text{film}} + \lambda_P^{\text{eq}} \lambda_{\text{film}}^{\text{eq}} (\chi_S - \xi_{\text{film}}) + \lambda_S \lambda_{\text{film}}^{\text{eq}} \chi_P} \quad (17)$$

During the cryo-supersonic air-quenching, the non-isothermal oxidation would have some special effects on transient conjugate heat transfer characteristics. Thus, in the case of the initial film thickness $\xi_0 = 0 \mu\text{m}$, the variations of the ECHTC at different radial positions with time are analyzed, and compared with the results under a non-oxidation condition, as shown in fig. 6. It can be found that the film growth makes the ECHTC at different radial positions decrease to a certain degree. But the variation ranges are relatively small (about 1-2 W/m²K) because the oxide film is extremely thin during the short-time oxidation. Simultaneously, one still can see that the growing oxide film does not obviously change the variation rule of the ECHTC with time.

To further investigate the effects of oxide film on transient conjugate heat transfer, the wall temperatures and the ECHTC under different initial film thickness $\xi_0 = 0 \mu\text{m}$, 100 μm , 200 μm , 300 μm , and 400 μm are analyzed. The effects of initial film thickness on the stagnation temperature profile and the radial distribution of the wall temperature at 50 seconds are shown in figs. 7 and 8, respectively. As presented in fig. 7, the stagnation temperature gradually increases with the increase of the initial film thickness, while the influence increases with time and then becomes stable. A similar pattern can be observed in the variation of the wall temperature with the initial film thickness given in fig. 8, and the corresponding influence decreases with the radial coordinate. In particular, the stagnation temperature increases linearly by about 5 K per 100 μm increase in initial film thickness.

Furthermore, the effects of initial film thickness on the stagnation ECHTC profile and the radial ECHTC distribution are shown in figs. 9 and 10, respectively. It is evident that the stagnation ECHTC, as well as the radial ECHTC, decreases with the increase of the initial film thickness on the whole. Especially the ECHTC in the stagnation region decreases linearly by about 55 W/m²K per 100 μm increase in initial film thickness. Compared with the pattern illustrated in fig. 8, the influence of initial film thickness on the radial ECHTC distribution is more complicated. This is largely due to the highly compressible supersonic flow in the near-wall region, which further leads to the viscous heating caused by the viscous dissipation, as demonstrated in fig. 10. Thus the radial ECHTC distribution in the near-wall region of super-

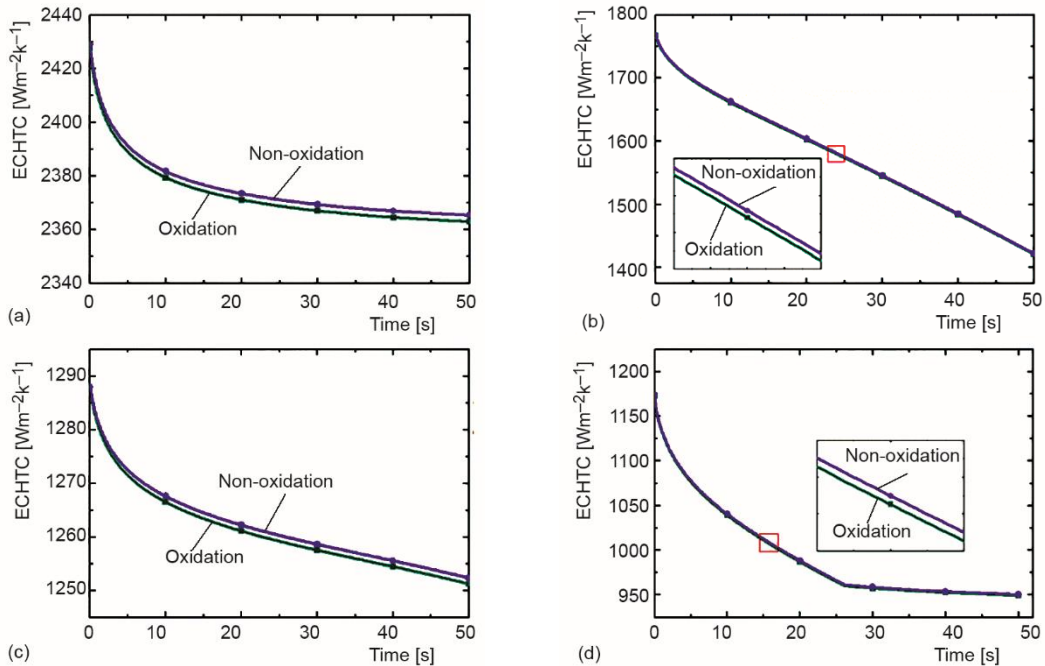


Figure 6. Variations of the ECHTC under oxidation and non-oxidation conditions; (a) $r = 0$ mm, (b) $r = 20$ mm, (c) $r = 40$ mm, and (d) $r = 60$ mm

sonic flow is significantly different from that of low subsonic flow without viscous dissipation. As the thermal resistance induced by the viscous heating is much larger than that of the oxide film, it may be concluded that the oxide film would have little impact on transient conjugate heat transfer when the near-wall velocity is higher.

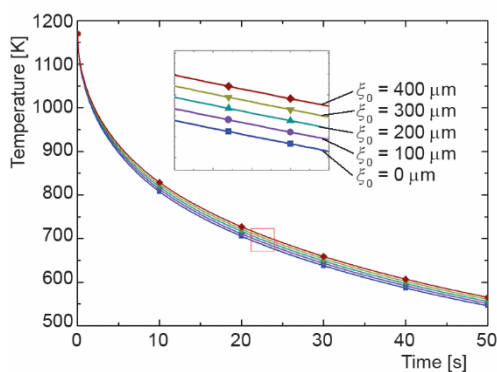


Figure 7. Effect of initial film thickness on the instantaneous temperature

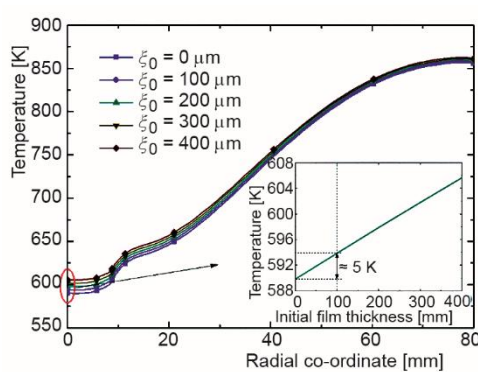


Figure 8. Effect of initial film thickness on the radial temperature (for color image see journal web site)

Conclusions

This research identifies the effects of instantaneous film growth and initial film thickness on transient conjugate heat transfer characteristics of the cryo-supersonic air-quen-

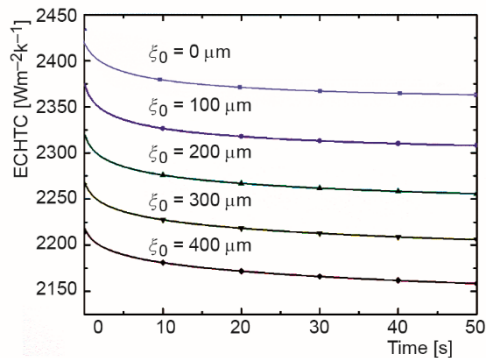


Figure 9. Effect of initial film thickness on the instantaneous ECHTC

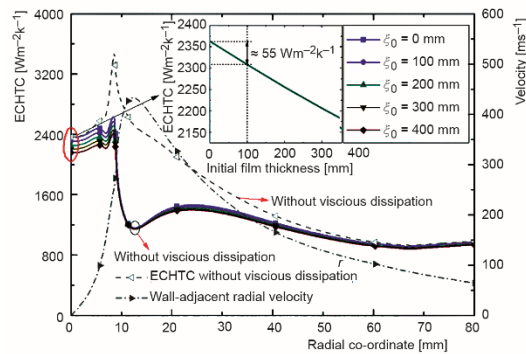


Figure 10. Effect of initial film thickness on the radial ECHTC (for color image see journal web site)

ching. The non-isothermal oxidation is determined by a double-layered oxidation kinetics model, while a unified formula is developed to efficiently solve the complex transient conjugate heat transfer. Good accuracy and reliability of the developed model have been validated, and the relative deviations between the numerical and experimental results are within 11%. Results show that the film growth makes the ECHTC decrease to a certain degree, but the variation range is relatively small (about 1-2 W/m²K¹) because the oxide film is extremely thin during the short-time oxidation. With the increase of the initial film thickness, the wall temperature increases, while the ECHTC decreases. In particular, the stagnation temperature increases linearly by about 5 K per 100 μm increase in film thickness, and the ECHTC in the stagnation region decreases linearly by about 55 W/m²K¹ per 100 μm increase in film thickness. More importantly, the oxide film would have little impact on transient conjugate heat transfer when the near-wall velocity is higher due to the effect of viscous dissipation.

Acknowledgment

This study was supported by the National Natural Science Foundation of China (51374127), the Innovative Research Team Fund of Education Department of Liaoning Province (LT2015014), and the Open Project Fund of Key Laboratory of Liaoning Province (USTLKFSY201713).

References

- [1] Goldstein, R. J., et al., Heat Transfer – a Review of 2005 Literature, *International Journal of Heat and Mass Transfer*, 53 (2010), 21-22, pp. 4397-4447
- [2] Olawale, J. O., et al., Forced-Air Cooling Quenching: A Novel Technique for Austempered Ductile Iron Production, *International Journal of Metalcasting*, 11 (2017), 3, pp. 568-580
- [3] Xiao, B. W., et al., An Experimental Study of Heat Transfer During Forced Air Convection, *Journal of Materials Engineering and Performance*, 20 (2011), 7, pp. 1264-1270
- [4] Köhler, C., et al., Influence of Oxide Scales on Heat Transfer in Secondary Cooling Zones in the Continuous Casting Process: Part I, Heat Transfer Through Hot-Oxidized Steel Surfaces Cooled by Spray-Water, *Steel Research*, 61 (1990), 7, pp. 295-301
- [5] Wendelstorf, R., et al., Effect of Oxide Layers on Spray Water Cooling Heat Transfer at High Surface Temperatures, *International Journal of Heat and Mass Transfer*, 51 (2008), 19-20, pp. 4892-4901
- [6] Tsukamoto, K., et al., On the Onset of Quench During Spray Cooling: The Significance of Oxide Layers, *Applied Thermal Engineering*, 179 (2020), 115682

- [7] Yang, J., et al., Numerical Study of Transient Conjugate Heat Transfer of the Cryo-Supersonic Air-Quenching Based on a Mach-Weighted Pressure-Based Method, *International Journal of Heat and Mass Transfer*, 134 (2019), May, pp. 586-599
- [8] Xu, H., et al., The Finite Volume Method for Evaluating the Wall Temperature Profiles of the Superheater and Reheater Tubes in Power Plant, *Applied Thermal Engineering*, 112 (2017), Feb., pp. 362-370
- [9] Qi, J., et al., Numerical Simulation of the Heat Transfer of Superheater Tubes in Power Plants Considering Oxide Scale, *International Journal of Heat and Mass Transfer*, 122 (2018), July, pp. 929-938
- [10] Li, Y. H., Sellars, C. M., Comparative Investigations of Interfacial Heat Transfer Behaviour During Hot Forging and Rolling of Steel with Oxide Scale Formation, *Journal of Materials Processing Technology*, 80-81 (1998), Aug., pp. 282-286
- [11] Wu, J. Q., et al., Interfacial Heat Transfer Under Mixed Lubrication condition for Metal Rolling: A Theoretical Calculation Study, *Applied Thermal Engineering*, 106 (2016), Aug., pp. 1002-1009
- [12] Hu, P., et al., Effect of Oxide Scale on Temperature-Dependent Interfacial Heat Transfer in Hot Stamping Process, *Journal of Materials Processing Technology*, 213 (2013), 9, pp. 1475-1483
- [13] Chabičovský, M., et al., Effects of Oxide Layer on Leidenfrost Temperature During Spray Cooling of Steel at High Temperatures, *International Journal of Heat and Mass Transfer*, 88 (2015), Sept., pp. 236-246
- [14] Fukuda, H., et al., Effects of Surface Conditions on Spray Cooling Characteristics, *ISIJ International*, 56 (2016), 4, pp. 628-636
- [15] Wikström, P., et al., The Influence of Oxide Scale on Heat Transfer During Reheating of Steel, *Steel Research International*, 79 (2008), 10, pp. 765-775
- [16] Yurek, G. J., et al., The Formation of Two-Phase Layered Scales on Pure Metals, *Oxidation of Metals*, 8 (1974), 5, pp. 265-281
- [17] Young, D. J., *High Temperature Oxidation and Corrosion of Metals*, Elsevier, New York, USA, 2016
- [18] Launder, B. E., Spalding, D. B., The Numerical Computation of Turbulent Flows, *Computer Methods in Applied Mechanics and Engineering*, 3 (1974), 2, pp. 269-289
- [19] Viegas, J. R., et al., On the Use of Wall Functions as Boundary Conditions for Two-Dimensional Separated Compressible Flows, Report No. AIAA-85-0180, Ames Research Center, Reno, USA, 1985
- [20] Manjunatha, S., et al., Effect of Thermal Radiation on Boundary Layer Flow and Heat Transfer of Dusty Fluid Over an Unsteady Stretching Sheet, *International Journal of Engineering Science*, 4 (2013), 4, pp. 36-48
- [21] Takeda, M., et al., Physical Properties of Iron-Oxide Scales on Si-Containing Steels at High Temperature, *Materials Transactions*, 50 (2009), 9, pp. 2242-2246